Draft version September 28, 2010
Preprint typeset using LaTeX style emulateapj v. 11/10/09

arXiv:1004.4249v2 [astro-ph.HE] 27 Sep 2010

ACCELERATION OF ULTRA-HIGH ENERGY COSMIC RAYS IN THE COLLIDING SHELLS OF BLAZARS AND GRBS: CONSTRAINTS FROM THE FERMI GAMMA RAY SPACE TELESCOPE

Charles D. Dermer[1] & Soebur Razzaque[1,2]
[1]Space Science Division, Code 7653, Naval Research Laboratory,
Washington, DC 20375-5352, USA and
[2]NRL/NRC Research Associate

(Received April 23, 2010)
Draft version September 28, 2010

ABSTRACT

Fermi Gamma ray Space Telescope measurements of spectra, variability time scale, and maximum photon energy give lower limits to the apparent jet powers and, through $\gamma\gamma$ opacity arguments, the bulk Lorentz factors of relativistic jets. The maximum cosmic-ray particle energy is limited by these two quantities in Fermi acceleration scenarios. Recent data are used to constrain the maximum energies of cosmic-ray protons and Fe nuclei accelerated in colliding shells of GRBs and blazars. The Fermi results indicate that Fe rather than protons are more likely to be accelerated to ultra-high energies in AGNs, whereas powerful GRBs can accelerate both protons and Fe to $\gtrsim 10^{20}$ eV. Emissivity of nonthermal radiation from radio galaxies and blazars is estimated from the First Fermi AGN Catalog, and shown to favor BL Lac objects and FR1 radio galaxies over flat spectrum radio quasars, FR2 radio galaxies, and long-duration GRBs as the sources of UHECRs.

Subject headings: cosmic rays – galaxies: active – galaxies: jets – gamma rays: galaxies – radiation mechanisms: nonthermal – shock waves

1. INTRODUCTION

Hillas (1984) pointed out an essential requirement for acceleration of ultra-high-energy cosmic rays (UHECRs), namely that the particle Larmor radius $r_{\rm L} \cong E/QB$ must be smaller than the size scale of the acceleration region. Here E is the particle energy, $Q = Ze$ is its charge, and B is the magnetic field in the acceleration zone. This limitation applies to Fermi acceleration scenarios where a particle gains energy while diffusing through a magnetized region. Additional limitations due, for example, to radiative losses or available time, further restrict the maximum energies and therefore the allowed sites of UHECR acceleration.

Two plausible classes of astrophysical accelerators of extragalactic UHECRs are active galactic nuclei (AGN) (Mannheim & Biermann 1989; Berezinsky et al. 2002) and gamma-ray bursts (GRBs) (Waxman 1995; Vietri 1995; Milgrom & Usov 1995) (see also Rachen & Mészáros 1998; Halzen & Hooper 2002; Dermer & Menon 2009), though other types of sources, including young, highly magnetized neutron stars (Ghisellini et al. 2008) and structure formation shocks (Inoue 2008) remain viable. The announcement by the Auger collaboration (2007) of anisotropy in the arrival directions of cosmic rays with energies $E \gtrsim 6\times 10^{19}$ eV, even given the reduced correlation in the latest data from the Pierre Auger Observatory (Abraham et al. 2009), is compatible with the production of UHECRs in many source classes, including GRBs and blazars. Because of the GZK effect involving photohadronic interactions of protons or ions with CMB radiation (Greisen 1966; Zatsepin & Kuz'min 1966; Stecker 1968), higher-energy cosmic rays with $E \gtrsim 10^{20}$ eV must be produced by sources located within distances $d \lesssim 100$ Mpc in order to reach us without losing significant energy (e.g., Nagano & Watson 2000; Harari et al. 2006).

The most powerful AGNs and long-duration GRBs are found far outside the GZK radius, at redshifts $z \gtrsim 0.1$. It is therefore of interest to re-examine Fermi acceleration requirements to determine if there are AGN and GRB sources with appropriate properties within the GZK radius. Here we make a detailed examination to justify a simple derivation of maximum particle energy relating apparent source power and bulk Lorentz factor Γ in the framework of Fermi acceleration in colliding shells. (Note that these arguments do not apply to non-Fermi type mechanisms, for example, electrodynamic acceleration in pulsar magnetospheres.) The derived limits are compared with values implied by Fermi data, yielding constraints on UHECR acceleration in these sources. We then use the First Fermi Large Area Telescope (LAT) AGN Catalog (1LAC) (Abdo et al. 2010a) to estimate the nonthermal emissivity of AGNs.

We find that the lower luminosity BL Lac objects and FR1 radio galaxies are more likely to be the sources of UHECRs than the rare, powerful flat spectrum radio quasars (FSRQs) and FR2 radio galaxies, and are more likely to accelerate Fe than protons to ultra-high energies. GRBs, on the other hand, can accelerate both protons and Fe nuclei to ultra-high energies, but are rare within the GZK volume.

2. MAXIMUM PARTICLE ENERGY IN COLLIDING SHELLS

The total comoving energy density u', including rest-mass and magnetic-field energy density, of a cold, isotropic relativistic wind with total wind power L and outflow Lorentz factor $\Gamma = 1/\sqrt{1-\beta^2}$ at radius r from the source is $u' = L/(4\pi r^2 \beta\Gamma^2 c)$. Primes here and below refer to quantities measured in the proper (comoving) frame of the radiating fluid. If a fraction ϵ_B of the to-

charles.dermer@nrl.navy.mil

tal energy density is in the form of magnetic-field energy density $u'_{B'} = B'^2/8\pi$, where B' is the magnetic field in the fluid frame, then $rB'\Gamma = \sqrt{2\epsilon_B L/\beta c}$, implying maximum particle energies $E_{max} \cong \beta\Gamma Q B' r' \cong \beta Q B' r$ (since the comoving size scale $r' \cong r/\Gamma$). Thus

$$E_{max} \cong \left(\frac{Ze}{\Gamma}\right)\sqrt{\frac{2\beta\epsilon_B L}{c}} \cong 2\times 10^{20} Z \frac{\sqrt{\epsilon_B \beta L_{46}/\epsilon_e}}{\Gamma}\ \mathrm{eV}\ , \tag{1}$$

where the nonthermal γ-ray luminosity $L_\gamma = 10^{46} L_{46}$ erg s^{-1} (e.g., Waxman 2004; Farrar & Gruzinov 2009), and we write $L_\gamma = \epsilon_e L$, where ϵ_e is the fraction of jet energy in electrons that is assumed to dominate the radiative γ-ray output. In general, $L_\gamma < L$, and $L_\gamma \ll L$ for radiatively inefficient flows. Besides giving the minimum apparent isotropic jet power, γ-ray observations give minimum values of Γ from $\gamma\gamma$ opacity arguments, allowing us to identify whether a given source is a plausible site for UHECR acceleration.

The estimate in eq. (1) does not, however, explain how a cold magnetohydrodynamic wind can transform directed kinetic energy to relativistic particles, which requires consideration of a specific model. Within the colliding shell framework (Rees & Meszaros 1994; Piran 1999), which is often invoked to explain the formation of spectra in GRBs and blazars, we can assess the conditions under which eq. (1) is valid. In this model, a central black hole is assumed to eject a slower shell a with coasting Lorentz factor $\Gamma_0 = \Gamma_a$ during explosion frame times $0 \le t_* \le \Delta t_{*a}$, followed by a faster shell b with $\Gamma_0 = \Gamma_b > \Gamma_a$ ejected at times $t_{*d} \le t_* \le t_* + \Delta t_{*,b}$, where t_{*d} is the stationary-frame delay time between the start of the ejections of shell a and b. The shell energies $\mathcal{E}_{a(b)}$ are related to their luminosities $L_{a(b)}$ through $\mathcal{E}_{a(b)} = L_{a(b)}\Delta t_{*a(b)}$.

The shells are assumed to collide after they reach their coasting phase. Neglecting shell spreading (which can be included by renormalizing the shell durations), and assuming that the event takes place sufficiently quickly so that we can approximate the shell density as constant during the duration of the collision, then simple kinematics shows that the collision radius r_{coll} and collision time $t_{*,coll}$ are given, in the limit $\Gamma_a \gg 1$, by

$$r_{coll} = ct_{*,coll} \cong \frac{2c\Gamma_a^2(t_{*d} - \Delta t_{*a})}{1-\rho_\Gamma^2}\ \ ,\ \ \rho_\Gamma \equiv \frac{\Gamma_a}{\Gamma_b} < 1\ . \tag{2}$$

The proper frame particle density in the shells is $n'_{a(b)} = L_{a(b)}/4\pi\Gamma^2_{a(b)} r^2 m_p c^3$ at radius r. Letting $\Gamma(\gg 1)$ denote the Lorentz factor of the shocked fluid, then the Lorentz factors of the forward f and reverse r shocks as measured in the shocked fluid frames are $\Gamma_{f(r)} \cong \Gamma\Gamma_{a(b)}(1-\beta_{a(b)}\beta) \to \frac{1}{2}(\Gamma/\Gamma_{a(b)} + \Gamma_{a(b)}/\Gamma)$ (Sari & Piran 1995). From the equality of kinetic energy densities at the contact discontinuity, we have

$$u \equiv \frac{n'_b}{n'_a} = \frac{\Gamma_f^2 - \Gamma_f}{\Gamma_r^2 - \Gamma_r} = \frac{\Gamma_a^2}{\Gamma_b^2}\frac{L_b}{L_a} = \rho_\Gamma^2 \frac{L_b}{L_a}\ . \tag{3}$$

Four asymptotic regimes can be identified, depending on whether the forward shock is relativistic (RFS) or nonrelativistic (NFS), and the reverse shock is relativistic (RRS) or nonrelativistic (NRS):

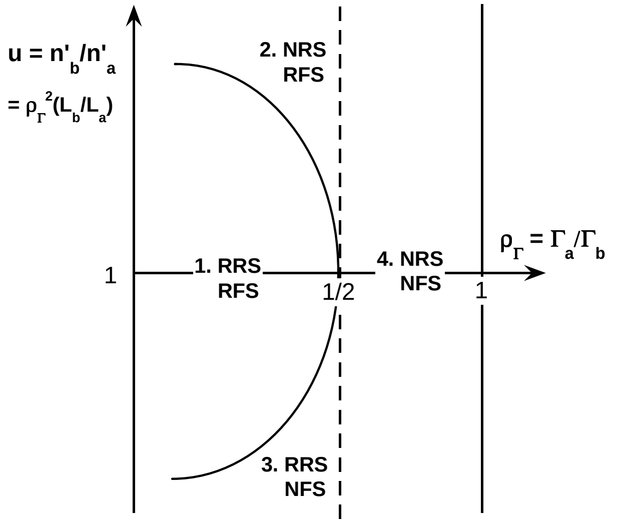

FIG. 1.— Different regimes in colliding shell interactions.

1. RRS ($\Gamma_r \gg 1$) and RFS ($\Gamma_f \gg 1$). This holds when $\Gamma_b \gg \Gamma \gg \Gamma_a$, implying

$$\Gamma \cong u^{1/4}\sqrt{\Gamma_a\Gamma_b}\ ,\ \Gamma_f = \frac{u^{1/4}}{2\sqrt{\rho_\Gamma}}\ ,\ \text{and}\ \Gamma_r = \frac{1}{2u^{1/4}\sqrt{\rho_\Gamma}} \tag{4}$$

when $\rho_\Gamma \ll \min(\sqrt{u}, 1/\sqrt{u})$.

2. NRS ($\Gamma_r - 1 \approx \beta_r^2/2$) and RFS, implying

$$\Gamma \cong \Gamma_b\ ,\ \Gamma_f = \frac{1}{2\rho_\Gamma}\ ,\ \text{and}\ \beta_r = \frac{1}{\sqrt{2u}\rho_\Gamma} \tag{5}$$

when $1/\sqrt{2u} \ll \rho_\Gamma \ll 1/2$ or $u \gg 1$. For this case, $L_b \gg L_a$.

3. RRS and NFS ($\Gamma_f - 1 \approx \beta_f^2/2$), implying

$$\Gamma \cong \Gamma_a\ ,\ \beta_f = \frac{1}{\rho_\Gamma}\sqrt{\frac{u}{2}}\ ,\ \text{and}\ \Gamma_r \cong \frac{1}{2\rho_\Gamma} \tag{6}$$

when $\sqrt{u/2} \ll \rho_\Gamma \ll 1/2$ or $u \ll 1$.

4. NRS and NFS, that is, $\beta_r \ll 1$ and $\beta_f \ll 1$, which takes place when $\Gamma_a \cong \Gamma_b \cong \Gamma$. Because $\rho_\Gamma \cong 1$, the duration of the interaction for this case may be sufficiently long to violate the assumption of constant shell density during the collision, though we formally treat it here.

Fig. 1 illustrates the various regimes in terms of the parameters u and ρ_Γ for which we derive maximum particle energies. The magnetic field B' in the shocked fluid is defined in the usual way (e.g., Sari et al. 1998), through a magnetic-field parameter ϵ_B, so that $B'_{f(r)} = \sqrt{32\pi m_p c^2 n'_{a(b)}\epsilon_{Bf(r)}(\Gamma^2_{f(r)} - \Gamma_{f(r)})}$. The duration of the flare from the forward shock is determined by the time $\Delta t'_a$ required for the forward shock to pass through shell a. The width of shell a in the frame of the shocked fluid is Δ'_a/Γ_f due to length contraction, where the proper frame width of shell a is $\Delta'_a = \Gamma\Delta_a(r)$. If $\bar\beta_f c$ is the speed of the FS, then $\bar\beta_f \cong 4\beta_f/3$ when $\Gamma_f - 1 \ll 1$, and $\bar\beta_f \cong 1$, $\bar\Gamma_f \cong \sqrt{2}\Gamma_f$, when $\Gamma_f \gg 1$. The duration of the event is also limited by the possibility that shell b dissipates its entire energy before the forward shock passes through shell a. Using similar reasoning for the reverse shock, we obtain the comoving timescales for the interactions at the forward and reverse shocks:

$$\Delta t'_{FS(RS)} = \min[\frac{\Gamma_{a(b)}\Delta_{a(b)}(r)}{\bar{\beta}_{f(r)}\Gamma_{f(r)}c}, \frac{\mathcal{E}_{b(a)}}{4\pi r^2 n'_{a(b)}\bar{\beta}_{f(r)}m_p c^3(\Gamma^2_{f(r)} - \Gamma_{f(r)})\Gamma}] \, . \tag{7}$$

Following the passage of the reverse and forward shocks through the shells, adiabatic expansion quickly ends subsequent acceleration and emission (Dermer 2008).

The maximum energy of particles accelerated at the forward and reverse shocks is given by $E_{max,f(r)} \cong Ze\Gamma B'_{f(r)}c\bar{\beta}_{f(r)}\Delta t'_{FS(RS)}$. The general expression can be written as

$$E_{max,f(r)} \cong \frac{Ze}{\Gamma}\sqrt{\frac{2\epsilon_{Bf(r)}L_{a(b)}}{c}}(\frac{\Gamma}{\Gamma_a})^2\sqrt{\frac{\Gamma_{f(r)}-1}{\Gamma_{f(r)}}} \times \frac{(1-\rho_\Gamma^2)\min[1, \frac{\mathcal{E}_{b(a)}}{\mathcal{E}_{a(b)}}\frac{\Gamma_{a(b)}}{\Gamma(\Gamma_{f(r)}-1)}]}{(t_{*d}-\Delta t_{*a})/\Delta t_{*a(b)}} \, . \tag{8}$$

The general expression for the maximum radiative efficiency giving the internal energy dissipated in the forward and reverse shocks can be written as

$$\mathcal{E}_{f(r)} = \min\left[\mathcal{E}_{a(b)}\frac{\Gamma(\Gamma_{f(r)}-1)}{\Gamma_{a(b)}} \, , \, \mathcal{E}_{b(a)}\right] . \tag{9}$$

For the different cases, we obtain the following results:

2.1. *Acceleration at the Forward Shock*

1. RRS and RFS.

$$E_{max,f} \cong \frac{Ze}{\Gamma}\sqrt{\frac{2\epsilon_{Bf}L_b}{c}}\,\frac{\min[1, \frac{2\mathcal{E}_b}{\mathcal{E}_a}\sqrt{\frac{L_b}{L_a}}]}{(t_{*d}-\Delta t_{*a})/\Delta t_{*a}} \, ,$$
$$\mathcal{E}_f = \min[\mathcal{E}_b, \frac{\mathcal{E}_a}{2}\sqrt{\frac{L_b}{L_a}}] \, . \tag{10}$$

2. NRS and RFS.

$$E_{max,f} \cong \frac{Ze}{\Gamma}\sqrt{\frac{2\epsilon_{Bf}L_b}{c}}\,\sqrt{\frac{L_a}{L_b}}\frac{\mathcal{E}_b}{\mathcal{E}_a}\frac{2\min[1, \mathcal{E}_a/2\rho_\Gamma^2\mathcal{E}_b]}{(t_{*d}-\Delta t_{*a})/\Delta t_{*a}} \, ,$$
$$\mathcal{E}_f = \min[\mathcal{E}_b, \mathcal{E}_a/2\rho_\Gamma^2] \, . \tag{11}$$

3. RRS and NFS.

$$E_{max,f} \cong \frac{Ze}{\Gamma}\sqrt{\frac{2\epsilon_{Bf}L_b}{c}}\,\frac{\min[1, 4(\mathcal{E}_b/\mathcal{E}_a)(L_a/L_b]}{(t_{*d}-\Delta t_{*a})/\Delta t_{*a}} \, ,$$
$$\mathcal{E}_f = \min[\mathcal{E}_a, 4\mathcal{E}_b(L_a/L_b)] \, , \tag{12}$$

4. NRS and NFS (also written for acceleration at the reverse shock).

$$E_{max,f(r)} \cong \frac{Ze}{\Gamma}\sqrt{\frac{2\epsilon_{Bf}L_{a(b)}}{c}} \times \frac{\beta_{f(r)}(1-\rho_\Gamma^2)}{\sqrt{2}}\,\frac{\min[1, 2\mathcal{E}_{b(a)}/\beta^2_{f(r)}\mathcal{E}_{a(b)}]}{(t_{*d}-\Delta t_{*a})/\Delta t_{*a(b)}} \, ,$$
$$\mathcal{E}_{f(r)} = \min[\beta^2_{f(r)}\mathcal{E}_{a(b)}/2, \mathcal{E}_{b(a)}] \, . \tag{13}$$

2.2. *Acceleration at the Reverse Shock*

1. RRS and RFS.

$$E_{max,r} \cong \frac{Ze}{\Gamma}\sqrt{\frac{2\epsilon_{Br}L_b}{c}}\,\frac{2\min[1, \mathcal{E}_b/2\mathcal{E}_a]}{(t_{*d}-\Delta t_{*a})/\Delta t_{*a}} \, ,$$
$$\mathcal{E}_r = \min[\mathcal{E}_a, \mathcal{E}_b/2] \, . \tag{14}$$

2. NRS and RFS.

$$E_{max,r} \cong \frac{Ze}{\Gamma}\sqrt{\frac{2\epsilon_{Br}L_b}{c}}\,\sqrt{\frac{L_a}{L_b}}\frac{2\min[1, \frac{\mathcal{E}_b/\mathcal{E}_a}{4u\rho_\Gamma^2}]}{(t_{*d}-\Delta t_{*a})/\Delta t_{*a}} \, ,$$
$$\mathcal{E}_r = \min[\mathcal{E}_a, \mathcal{E}_b/(2u\rho_\Gamma^2)] \, , \tag{15}$$

noting that $u\rho_\Gamma^2 \gg 1$ for this case.

3. RRS and NFS.

$$E_{max,r} \cong \frac{Ze}{\Gamma}\sqrt{\frac{2\epsilon_{Br}L_b}{c}}\,\frac{\min[1, 2\mathcal{E}_a/\mathcal{E}_b]}{(t_{*d}-\Delta t_{*a})/\Delta t_{*a}} \, ,$$
$$\mathcal{E}_r = \min[\mathcal{E}_a, \mathcal{E}_b/2] \, . \tag{16}$$

4. NRS and NFS, given by eq. (13).

3. LIMITATIONS ON UHECR ACCELERATION

The maximum particle energy for the various cases is always proportional to the umbrella function, eq. (1), derived from elementary principles, but multiplied by a coefficient $\lesssim \mathcal{O}(1)$. The ability of a shell collision to accelerate particles to the highest energies is conditioned on very specific behaviors of the shells, namely that the second shell is much faster than the first ($\rho_\Gamma \gg 1$), and that the time t_{*d} between shell ejections is a small factor larger than the duration Δt_{*a} of the event forming shell a (as expressed by the term $(t_{*d} - \Delta t_{*a})/\Delta t_{*a}$ in the denominators of eqs. (10) – (16)). The most favorable regime for particle acceleration to the highest energies occurs for the case of a RRS and RFS when the energies and luminosities of the two shells are about equal. This also gives the highest radiative efficiencies. The main requirement is a large contrast between the Lorentz factors of the two shells (Beloborodov 2000; Kumar & Piran 2000).

The highest radiative efficiency coincides with approximately equal energies and luminosities for the cases of a RRS and RFS, and a RRS and NFS. In the case of a NRS and RFS, where $L_b \gg L_a$ is required for validity of this asymptote, a much larger energy in shell b than shell a is required for maximum radiative efficiency at the reverse shock, as shown by eq. (15). Energy dissipation in this case would, however, more likely be dominated by the forward shock. Kinematic limitations ensure that the radiative efficiency is poor for dissipation at either the forward or reverse shocks for the case of a NRS and NFS, eq. (13), depending on the precise energies in each of the shells.

Supposing that the engines of GRBs and blazars or, for that matter, microquasars, eject shells with such properties (which is necessary in the case of GRBs to explain their high γ-ray radiative efficiency in an internal shock scenario; cf. Ioka et al. 2006), then we can construct a diagram illustrating the viability of various sources to accelerate UHECRs. In Fig. 2 we plot apparent luminosity as a function of Lorentz factor for the acceleration of 10^{20} eV protons (heavy solid curve) and Fe nuclei (heavy dot-dashed curve), from eq. (1). Note that we plot this equation to nonrelativistic values of Γ, which is outside the regime where we have considered its validity in a colliding shell scenario. Sources above these curves can in principle accelerate UHECRs. The acceleration rate in Fermi scenarios is governed by the Larmor timescale, so that the acceleration timescale $t'_{acc} = \phi r'/c = \phi E'/ZeB'c$, and $\phi \gtrsim 1$. Incidentally, the requirement that t'_{acc} is smaller than the available time $t'_{ava} = \Gamma t_v/(1+z)$, where t_v is the measured variability timescale, essentially recovers eq. (1) when $\phi = 1$ and $r \cong \Gamma^2 c t_v/(1+z)$. This shows that eq. (1) is a restatement of the Hillas condition by relating B to L and $r_{\rm L}$ to t_v.

Maximum particle energy is also limited by the requirement that (i) t'_{acc} is shorter than the synchrotron energy-loss timescale t'_{syn} (e.g., Guilbert et al. 1983). We can also consider the (less restrictive) condition (ii) $t'_{syn} > t'_{ava}$, so that particles do not significantly cool during the available time. Writing the comoving magnetic field $u'_B = \epsilon_B L_\gamma/(\epsilon_e 4\pi r^2\Gamma^2 c)$ and $E_{20} = E/10^{20}$eV, the former constraint becomes

$$\frac{E_{max,i}}{m_p c^2} \lesssim \Gamma^{5/2}\Big(\frac{A^2}{Z^{3/2}}\Big)\Big(\frac{m_p}{m_e}\Big)\sqrt{\frac{6\pi e c t_v}{\phi\sigma_{\rm T}(1+z)}}\;\Big(\frac{\beta\epsilon_e c}{2\epsilon_B L_\gamma}\Big)^{1/4}\;, \tag{17}$$

where Am_p is the particle mass, implying

$$L_{\gamma,i}(\text{erg s}^{-1}) \lesssim \frac{2\times10^{32}\Gamma^{10}}{E_{20}^4}\;\frac{t_v^2({\rm s})}{\phi^2(1+z)^2}\Big(\frac{A^8}{Z^6}\Big)\;\Big(\frac{\beta\epsilon_e}{\epsilon_B}\Big)\;, \tag{18}$$

For the second case,

$$\frac{E_{max,ii}}{m_p c^2} \cong 3\pi\Big(\frac{A}{Z}\Big)^4\Big(\frac{m_p}{m_e}\Big)^3\;\frac{\beta\epsilon_e}{\epsilon_B}\;\frac{(m_e c^2)}{\sigma_{\rm T}L_\gamma}\;\frac{c^2\Gamma^6 t_v}{1+z}\;, \tag{19}$$

implying

$$L_{\gamma,ii}(\text{erg s}^{-1}) \lesssim \frac{6\times10^{38}\Gamma^6 t_v({\rm s})}{E_{20}(1+z)}\;\Big(\frac{A}{Z}\Big)^4\;\Big(\frac{\beta\epsilon_e}{\epsilon_B}\Big)\;. \tag{20}$$

The restrictions implied by eqs. (18) and (20) are shown by the dashed and dotted lines, respectively, in Fig. 2, for parameters characteristic of UHECR proton acceleration to 10^{20} eV in blazars and GRBs. Here $\epsilon_e/\epsilon_B = 1, \phi = 10$, and $t_v = 10^4$ s and 10 ms, and $\Gamma = 10$ and 10^3, for blazars and GRBs, respectively. We also plot data for various sources observed with Fermi and ground-based γ-ray telescopes. In all cases except Centaurus A, Γ_{min} is derived from $\gamma\gamma$ opacity arguments, with the apparent γ-ray luminosity giving the minimum source luminosity. The inference of Γ_{min} from $\gamma\gamma$ opacity arguments is model dependent, with the determination of Γ_{min} dependent on assumptions about target-photon anisotropy, relationship between variability time and emission region size scale, photon escape probability, and the dynamic state of the emitting plasma (e.g., Ackermann et al. 2010; Granot et al. 2008). Even so, the strong Γ-dependence of comoving photon energy density $u'_\gamma \propto \Gamma^{-6}$ makes it unlikely that the actual value of Γ_{min} differ by more than a factor of ≈ 2 from the value derived through simple $\gamma\gamma$ arguments.

The long-duration GRB 080916C (Abdo et al. 2009a) and the short-duration GRB 090510A (Ackermann et al. 2010) have $\Gamma_{min} \approx 10^3$ and $L_\gamma \approx 10^{53}$ erg s^{-1}. GRB 090902B, with $\Gamma_{min} \approx 10^3$ and $L_\gamma \approx 10^{54}$ erg s^{-1} between 6 and 13 s after the trigger time (Abdo et al. 2009b), would cluster in the same regime. For 3C 454.3, $\Gamma_{min} \approx 8$ and $L_\gamma \approx 5\times10^{48}$ erg s^{-1} (Abdo et al. 2009c). In the case of NGC 1275, $L_\gamma \approx 10^{42}$ erg s^{-1} and the Doppler factor (and therefore Γ) is $\gtrsim 2$ (Abdo et al. 2009d). For PKS 2155-304, a BL Lac object, we use the results of Finke et al. (2008) for the giant flares of 2006 July (Aharonian et al. 2007), which employs a synchrotron self-Compton model with $\gamma\gamma$ absorption and various EBL models to derive $\Gamma \approx 100$. Note that the absolute jet powers derived there can be much less than the apparent jet power that enters into the acceleration constraint defined by HESS measurements of its apparent isotropic γ-ray luminosity $L_\gamma \approx 3\times10^{46}$ erg s^{-1}.

Finally, we consider the case of the FR1 radio galaxy Cen A, the only one of the sources shown in Fig. 1 that is within the GZK radius. It is of special interest, of course, because of the clustering of the arrival directions of several UHECRs towards Cen A (Auger collaboration 2007; Moskalenko et al. 2009; Abraham et al. 2009), and early speculations that it could be a dominant source of UHECRs (Piran & Farrar 2001). Because its jet is pointed away from our line of sight, the jet luminosity and Γ factor of Cen A can only be indirectly inferred (Kraft et al. 2002). One way is to assume that the energy of the radio lobes are powered by the jets, and use synchrotron theory and lobe dynamics to infer total energy and lifetime. Values between $\approx 10^{42} - 10^{43}$ erg s^{-1} are inferred (Hardcastle et al. 2009), with jet beaming and episodes of intense outbursts arguably capable of allowing the jet to reach apparent powers sufficient to accelerate UHECR protons (Dermer et al. 2009).

Deceleration of relativistic shells by the surrounding medium generates a relativistic external forward shock and a relativistic/non-relativistic reverse shock. The time scale for deceleration depends on the apparent isotropic kinetic energy of the merged shells $E_{\rm k,iso}$, the bulk Lorentz factor Γ_0 and the density of the surrounding medium n, given by $t_{\rm dec} \cong (1+z)(3E_{\rm k,iso}/[32\pi m_p c^5 n\Gamma_0^8])^{1/3} \approx 1.9(1+z)n^{-1/3}E_{55}^{1/3}\Gamma_3^{-8/3}$ s. The subsequent evolution of the blast wave is described by the Blandford & McKee (1976) self-similar solutions. Acceleration of cosmic rays to maximum energies in the forward shock takes place during the deceleration time, and similar to eq. (1) we can write from $t_{\rm dec} = t_{\rm acc}$

$$\begin{aligned} E_{\rm max} &\cong \frac{Ze}{\phi(1+z)}\frac{\Gamma_0^{1/3}}{2^{17/12}}(9\pi E_{\rm k,iso}^2\epsilon_B^3 n m_p c^2)^{1/6} \\ &\approx 1.4\times10^{21}\frac{Z}{\phi(1+z)}n^{1/6}\epsilon_B^{1/2}E_{55}^{1/3}\Gamma_3^{1/3}\ \text{eV}. \end{aligned} \tag{21}$$

The corresponding constraint on the apparent isotropic kinetic energy and bulk Lorentz factor to accelerate particles to 10^{20} eV is

$$E_{\rm k,iso} \approx 3.4 \times 10^{54} \frac{\phi^3 (1+z)^3}{Z^3 \epsilon_B^{3/2} n^{1/2} \Gamma_0} \text{ erg.} \tag{22}$$

This constraint is satisfied by most long-duration GRBs to accelerate both protons and Fe nuclei, and by FSRQ blazars (depending in detail on the energy of the blazar flare and density of decelerating medium) to accelerate Fe nuclei.

4. DISCUSSION

Fig. 2 shows that the short- and long-duration GRBs for which Fermi observations give both L_γ and Γ_{min} easily satisfy the luminosity requirements to accelerate UHECR protons or ions. After considering the specific parameter values that enter into eqs. (18) and (20), one finds that the additional constraints imposed by the synchrotron cooling rate are not severe either for blazars or GRBs. One difficulty for arguing that GRBs are the sources of UHECRs is their rarity within the GZK radius. Only if the intergalactic magnetic field is sufficiently strong ($\sim$ nG with Mpc scales for magnetic-field reversals) to disperse the arrival time of the UHECRs, but not so strong to erase their inhomogeneous arrival directions, can long and short GRBs be plausible UHECR candidates (Razzaque et al. 2009). More complicated magnetic field geometries can also relieve this problem (Kashti & Waxman 2008). A further difficulty accompanying the large Γ values and correspondingly dilute comoving photon energy densities implied by the Fermi results on GRBs is that photohadronic processes are suppressed. Intermediate neutron production with the escape of ultra-high energy neutrons that subsequently decay to form UHECRs was proposed as a principal mechanism (Atoyan & Dermer 2003) to circumvent the problem of the escape of UHECR ions. Such escape is problematic in a bursting source because the strong flux of ions will generate a shock that causes the ions to lose energy as they leave the GRB. (Murase & Beacom 2010). Future Fermi observations will reveal whether there is a large population of low Γ-factor GRBs, or if another class of GRBs, such as low-luminosity GRBs (Murase et al. 2006; Wang et al. 2007; Liang et al. 2007), can make the UHECRs.

From the 1LAC catalog (Abdo et al. 2010a), we can make a diagram, Fig. 3, of the volume-averaged nonthermal γ-ray luminosity density (or emissivity). Here we use the time-averaged 100 MeV – 100 GeV luminosity measured over eleven months, and divide by the volume $4\pi d^3/3$ associated with the proper distance d of the individual sources to make a cumulative emissivity for different classes of γ-ray galaxies. The volume-averaged emissivity, unlike the source density, is independent of the beaming factor. The cumulative emissivities are shown separately for BL Lac objects, FSRQs, misaligned AGNs, and non-AGN star-forming and starburst galaxies, including M82 and NGC 253 (Abdo et al. 2010b), as well as NGC 4945 reported in the 1LAC. NGC 4945 is classified here as a starburst, though it also contains a Seyfert nucleus. The misaligned AGNs consist of 11 sources, including seven FR1 radio galaxies and four FR2 radio sources. The FR1 galaxies are Cen A, M87, NGC 1275, NGC 6251, NGC 1218 (3C 78), and PKS 0625-35 (Abdo et al. 2010a). The FR2 objects consist of two radio galaxies, 3C 111 and PKS 0943-76, and two steep spectrum radio quasars, 3C 207 and 3C 380.

For comparison with the cumulative emissivity, the fiducial luminosity-density value of $\approx 10^{44}$ erg Mpc^{-3} yr^{-1} that is needed for classes of sources to energize UHECRs against GZK losses (Waxman & Bahcall 1999) is shown. What is obvious from Fig. 3 is that FSRQs do not have sufficient emissivity to power the UHECRs under the assumption that the γ-ray luminosity is a good measure of the UHECR power. A much larger energy release in UHECRs than γ rays is possible, but even so, FSRQs are absent within the GZK radius, and FR2 radio galaxies, which are the putative parent population of FSRQs under the unification hypothesis (Urry & Padovani 1995), are only found at distances $\gtrsim 100$ Mpc (Moskalenko et al. 2009). Pictor A is the closest FR2 radio galaxy at $z = 0.035$, and Cygnus A is at $z = 0.056$; neither has yet been reported as Fermi LAT sources. The redshifts of the detected FR2 radio galaxies 3C 111 and PKS 0943-76 are 0.049, and 0.27, respectively.

The comparison is more favorable for BL Lac objects which, as indicated by Fig. 3, have the necessary nonthermal power to energize UHECRs. The ones detected at GeV energies are still outside the GZK radius, though the famous TeV (and GeV) blazars Mrk 421 and Mrk 501 reside, at ≈ 130 Mpc, just outside it (see also Takami & Sato 2009, for a discussion of the space density of putative UHECR sources). The unification hypothesis would then suggest that many FR1 radio galaxies are found at closer distances, including misaligned galaxies detected at γ-ray energies. Indeed FR1 galaxies detected at GeV energies are found within the GZK radius, as shown by the misaligned AGNs in Fig. 3. Misalignment means that the γ-ray luminosity when viewed directly along the jet is probably much larger than the luminosity measured with Fermi. NGC 1275 has apparent γ-ray luminosity of $\approx 10^{44}$ erg s^{-1} and, at a distance of ≈ 75 Mpc, falls within the GZK radius (Abdo et al. 2009d). It is variable at γ-ray energies, indicating that much of its γ ray flux is probably associated with a jet. Moreover, it is a compact symmetric object, with transient outbursts with durations of $\approx 10^4 - 10^5$ yrs during which conditions are more favorable for UHECR acceleration (Horiuchi & Takami 2009). The variability is not short enough to give Γ_{min} from $\gamma\gamma$ arguments, though modeling results and observations of apparent superluminal motion suggest mildly relativistic Lorentz factors. By comparison, Cen A has relatively small apparent γ-ray lobe and core luminosities, each amounting to $\approx 10^{41}$ erg s^{-1}, but its emissivity is large due to its proximity.

The star-forming and starburst galaxies are abundant within the GZK radius, and have substantial γ-ray emissivity, which is more than adequate to account for the power needed to accelerate UHECRs. Where this source class falters, however, is in the low individual GeV – TeV γ-ray luminosities, representing $\approx 3 \times 10^{39}$ erg s^{-1} for the Milky Way, and $\sim 10^{40}$ erg s^{-1} for the luminous starbursts (Abdo et al. 2010b). Fermi acceleration of UHECRs with such low powers is, as seen from Fig. 2, not feasible. Furthermore, the lack of reported detection of γ-ray emission from clusters of galaxies weakens the case for UHECR acceleration in structure-formation shocks.

Long-duration GRBs have apparent γ-ray luminosities far greater than needed to accelerate cosmic-ray protons or ions to $E \gtrsim 10^{20}$ eV, as shown in Fig. 2. Their time-averaged photon luminosity density is, however, insufficient to power UHECRs within the GZK radius unless the typical baryon loading in GRBs, representing the ratio of energy in cosmic rays to that radiated as photons, is $\gg 1$. Estimates for the local ($z \ll 1$) luminosity density, based on the luminosity function and local event rate density of long-duration GRBs, range from $\approx 6\times10^{42}(\Delta t/20\text{ s})$ erg Mpc^{-3} yr^{-1} Schmidt (2001, though without using GRB redshift information), to $\approx 2\times10^{44}(\Delta t/10\text{ s})$ erg Mpc^{-3} yr^{-1} (Wanderman & Piran 2010), where Δt is the mean duration of long GRBs in the explosion frame. A local luminosity density of $(5-8)\times10^{42}(\Delta t/10\text{ s})$ erg Mpc^{-3} yr^{-1} is derived in the treatment of Guetta et al. (2005) and the luminosity function of Liang et al. (2007) implies a local luminosity density of $\approx 2\times10^{43}(\Delta t/10\text{ s})$ erg Mpc^{-3} yr^{-1}. Based on a physical model of GRB jets, Le & Dermer (2007) calculate a long duration GRB density of $(3-4)\times10^{43}$ erg Mpc^{-3} yr^{-1}, assuming $\Delta t = 10$ s.

By comparison with the nonthermal luminosity density of long-duration GRBs, that of FR1 radio galaxies and BL Lac objects within the GZK radius is at least $1-2$ orders of magnitude larger (Fig. 3). If the comparison is with the nonthermal emission emitted in the GeV/LAT range rather than at MeV energies, which could be thermal or photospheric emission, then the required baryon loading must be an order of magnitude larger (Eichler et al. 2010). The local photon luminosity densities of the short hard GRBs (e.g., Guetta 2006) or low luminosity GRBs (Wang et al. 2007; Liang et al. 2007; Murase et al. 2008) can also be comparable to the emissivity from long-duration GRBs, though with a larger local space density and smaller energy release per event.

5. CONCLUSIONS

Fermi observations shown in Fig. 3 indicate that FR1 radio galaxies and misaligned BL Lac objects located within the GZK radius have sufficient emissivity to power the UHECRs. With typical Lorentz factors $\approx 2-10$, and apparent jet powers $\approx 10^{44}-10^{45}$ erg s^{-1} (which could exceed 10^{46} erg s^{-1} and large Lorentz factors during flaring episodes), Fig. 2 shows that acceleration of Fe nuclei in FR1 radio galaxies is possible in colliding shells made in the jets of these galaxies. Given the favorable circumstances needed for colliding shells to accelerate UHECRs, including large Lorentz factor contrast and short times between shell ejections, the acceleration of protons is less likely. The $L-\Gamma$ constraint is unfavorable for UHECR acceleration at sites with low apparent luminosity, such as starburst galaxies or the lobes of radio galaxies.

Long-duration GRBs have sufficient power to accelerate cosmic rays to ultra-high energies, but their local photon luminosity density in photons, $\sim 10^{43}-10^{44}$ erg Mpc^{-3} yr^{-1}, implies comparable or large baryon loading in most models for UHECR acceleration. When compared with the clearly nonthermal Fermi LAT flux, the required baryon-loading becomes significant, as shown by Eichler et al. (2010). The local nonthermal luminosity density of FR1 radio galaxies and BL Lac objects by far dominates that of GRBs, especially when compared only with the LAT fluxes from GRBs and blazars. This circumstance favors UHECR acceleration by the supermassive black-hole engines in radio galaxies and blazars, provided that UHECRs are predominantly Fe ions.

We thank R. Blandford, C. C. Cheung, D. Eichler, and J. Finke for helpful discussions and correspondence, and acknowledge useful comments by the referee. This work is supported by the Office of Naval Research and NASA Fermi Guest Investigator grants NNG 10PK07I and NNG 10PE02I.

REFERENCES

Abdo, A. A., et al. 2009a, Science, 323, 1688 (GRB 080916C)
Abdo, A. A., et al. 2009b, ApJ, 706, L138 (GRB 090902B)
Abdo, A. A., et al. 2009c, ApJ, 699, 817 (3C454.3)
Abdo, A. A., et al. 2009d, ApJ, 699, 31 (NGC 1275)
Abdo, A. A., et al. 2010a, ApJ, 715, 429 ApJ, 715, 429 (1LAC)
Abdo, A. A., et al. 2010b, ApJ, 709, L152 (starbursts)
Ackermann, M., et al. 2010, ApJ, 716, 1178 (GRB 090510A)
The Pierre Auger Collaboration, J. Abraham et al., 2007, Science, 318, 938
The Pierre Auger Collaboration: J. Abraham, et al. 2009, arXiv:0906.2347
Aharonian, F., et al. 2007, ApJ, 664, L71
Atoyan, A. M., & Dermer, C. D. 2003, ApJ, 586, 79
Beloborodov, A. M. 2000, ApJ, 539, L25
Berezinsky, V., Gazizov, A. Z., & Grigorieva, S. I. 2002, arXiv:astro-ph/0210095
Blandford, R. D., & McKee, C. F. 1976, Physics of Fluids, 19, 1130
Dermer, C. D. 2008, ApJ, 684, 430
Dermer, C. D., & Menon, G. 2009, High Energy Radiation from Black Holes (Princeton University Press)
Dermer, C. D., Razzaque, S., Finke, J. D., & Atoyan, A. 2009, New Journal of Physics, 11, 065016
Eichler, D., Guetta, D., & Pohl, M. 2010, arXiv:1007.3742
Fanaroff, B. L., & Riley, J. M. 1974, MNRAS, 167, 31P
Farrar, G. R., & Gruzinov, A. 2009, ApJ, 693, 329
Finke, J. D., Dermer, C. D., & Böttcher, M. 2008, ApJ, 686, 181
Ghisellini, G., Ghirlanda, G., Tavecchio, F., Fraternali, F., & Pareschi, G. 2008, MNRAS, 390, L88
Granot, J., Cohen-Tanugi, J., & do Couto e Silva, E. 2008, ApJ, 677, 92
Greisen, K. 1966, Physical Review Letters, 16, 748
Guetta, D., Piran, T., & Waxman, E. 2005, ApJ, 619, 412
Guetta, D. 2006, Nuovo Cimento B Serie, 121, 1061
Guilbert, P. W., Fabian, A. C., & Rees, M. J. 1983, MNRAS, 205, 593
Halzen, F., & Hooper, D. 2002, Reports of Progress in Physics, 65, 1025
Harari, D., Mollerach, S., & Roulet, E. 2006, JCAP, 11, 12
Hardcastle, M. J., Cheung, C. C., Feain, I. J., & Stawarz, Ł. 2009, MNRAS, 393, 1041
Hillas, A. M. 1984, ARA&A, 22, 425
Horiuchi, S., & Takami, H., 2009, preprint
Inoue, S. 2008, Journal of Physics Conference Series, 120, 062001
Ioka, K., Toma, K., Yamazaki, R., & Nakamura, T. 2006, A&A, 458, 7
Kashti, T., & Waxman, E. 2008, JCAP, 5, 6
Kraft, R. P., Forman, W. R., Jones, C., Murray, S. S., Hardcastle, M. J., & Worrall, D. M. 2002, ApJ, 569, 54
Kumar, P., & Piran, T. 2000, ApJ, 535, 152
Le, T., & Dermer, C. D. 2007, ApJ, 661, 394
Liang, E., Zhang, B., Virgili, F., & Dai, Z. G. 2007, ApJ, 662, 1111
Mannheim, K., & Biermann, P. L. 1989, A&A, 221, 211

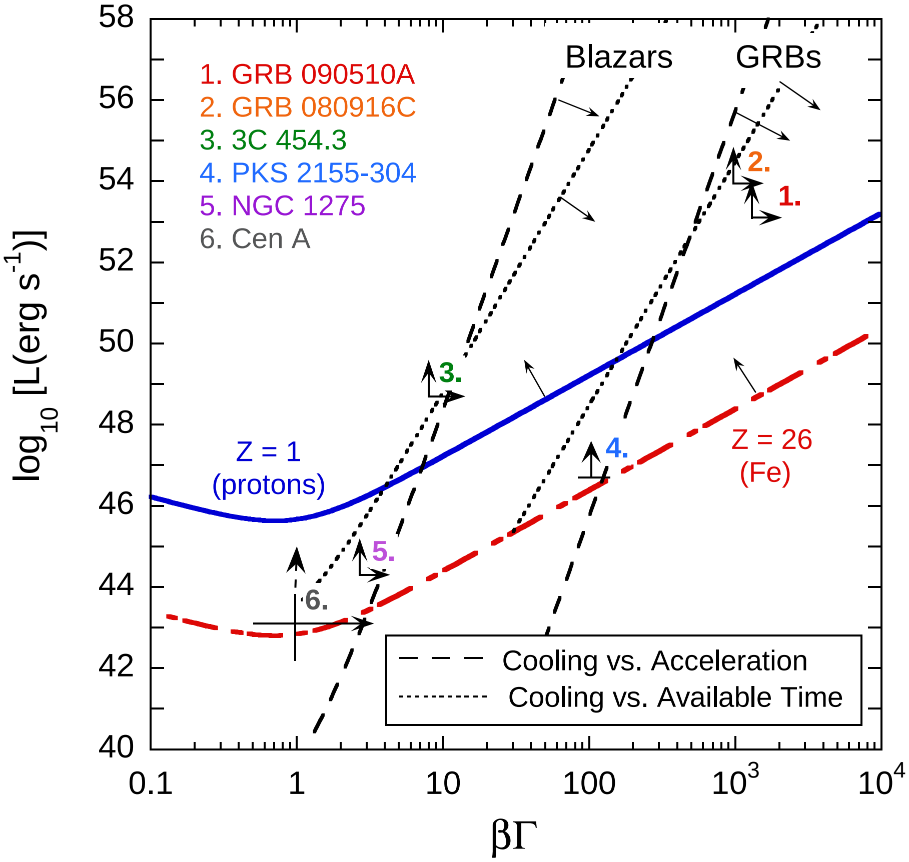

Fig. 2.— Sources with jet Lorentz factor $\Gamma = \sqrt{\beta^2\Gamma^2 + 1}$ must have jet power L exceeding the heavy solid and dot-dashed curves to accelerate protons and Fe, respectively, to $E = 10^{20}$ eV, from eq. (1). Upper limits to L as a function of Γ for acceleration of UHECR protons to 10^{20} eV in blazars and GRBs are given by the dashed lines due to competition between synchrotron losses and acceleration, and by the dotted lines when comparing synchrotron losses and available time. Here we use variability time $t_v = 10^4$ s and $z \ll 1$ for blazars, and $t_v = 10$ ms and $z = 1$ for GRBs, as labeled, with $\phi = 10$ in both cases. Scalings for different values of t_v, Γ, z, and ϕ are given by eqs. (18) and (20).

Milgrom, M., & Usov, V. 1995, ApJ, 449, L37
Moskalenko, I. V., Stawarz, L., Porter, T. A., & Cheung, C. C. 2009, ApJ, 693, 1261
Murase, K., & Beacom, J. F. 2010, PRD, in press, arXiv:1002.3980
Murase, K., Ioka, K., Nagataki, S., & Nakamura, T. 2008, Phys. Rev. D, 78, 023005
Murase, K., Ioka, K., Nagataki, S., & Nakamura, T. 2006, ApJ, 651, L5
Nagano, M., & Watson, A. A. 2000, Reviews of Modern Physics, 72, 689
Piran, T. 1999, Phys. Rep., 314, 575
Piran, T., & Farrar, G. R. 2001, 20th Texas Symposium on relativistic astrophysics, 586, 850
Rachen, J. P., & Mészáros, P. 1998, Phys. Rev. D, 58, 123005
Razzaque, S., Dermer, C. D., & Finke, J. D. 2010, Open Astronomy Journal, III, 150 (arXiv:0908.0513)
Rees, M. J., & Meszaros, P. 1994, ApJ, 430, L93
Sari, R., & Piran, T. 1995, ApJ, 455, L143
Sari, R., Piran, T., & Narayan, R. 1998, ApJ, 497, L17
Schmidt, M. 2001, ApJ, 552, 36
Stecker, F. W. 1968, Physical Review Letters, 21, 1016
Takami, H., & Sato, K. 2009, Astroparticle Physics, 30, 306
Urry, C. M., & Padovani, P. 1995, PASP, 107, 803
Vietri, M. 1995, ApJ, 453, 883
Wanderman, D., & Piran, T. 2010, MNRAS, 406, 1944
Wang, X.-Y., Razzaque, S., Mészáros, P., & Dai, Z.-G. 2007, Phys. Rev. D, 76, 083009
Waxman, E. 1995, Phys. Rev. Lett., 75, 386
Waxman, E. 2004, New Journal of Physics, 6, 140
Waxman, E., & Bahcall, J. 1999, Phys. Rev. D, 59, 023002
Zatsepin, G. T., & Kuz'min, V. A. 1966, Soviet Journal of Experimental and Theoretical Physics Letters, 4, 78

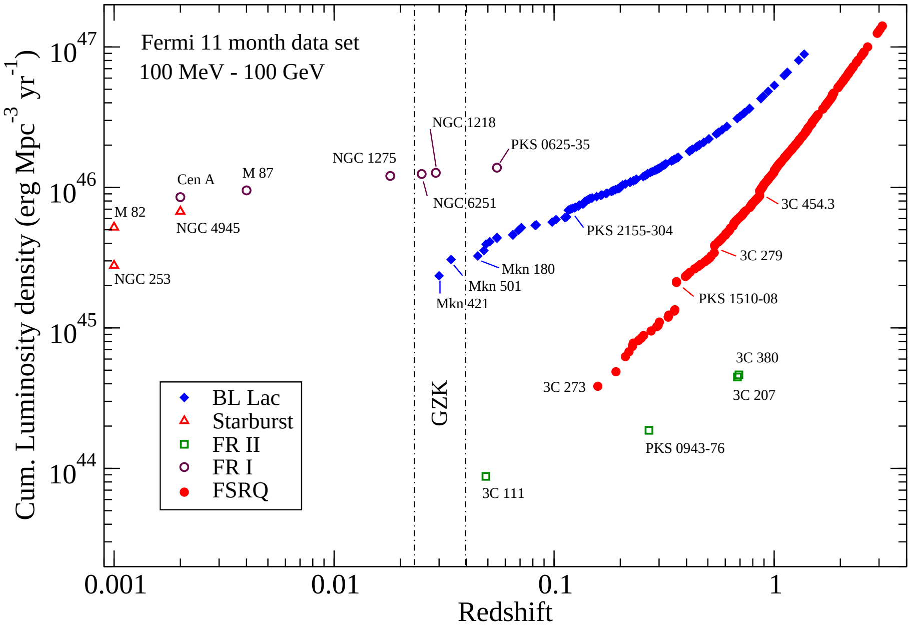

FIG. 3.— Nonthermal luminosity density of different classes of γ-ray galaxies detected with Fermi. Here we show cumulative emissivities for FSRQ, BL Lacs, FR1 and FR2 radio galaxies, and star-forming galaxies. The band between $\approx$ 100 and 200 Mpc labeled "GZK" represents the outer perimeter from which sources of UHECRs with energies $\gtrsim 10^{20}$ eV can originate.